# Current Sensorless Equalization Strategy for Single-Switch Voltage Equalizer Using Multi-Stacked Buck-Boost Converters for Photovoltaic Modules under Partial Shading

Masatoshi Uno, *Member, IEEE*, and Akio Kukita

***Abstract*— Differential power processing converters and voltage equalizers have been proposed and used for photovoltaic (PV) string comprising multiple modules/substrings connected in series in order to preclude negative influences of partial shading. The single-switch voltage equalizer using multi-stacked buck-boost converters can significantly reduce the necessary switch count compared to that of conventional topologies, achieving simplified circuitry. However, multiple current sensors are necessary for this single-switch equalizer to effectively perform equalization. In this paper, a current sensorless equalization technique ($\Delta V$-controlled equalization) is presented. The equalization strategy using the $\Delta V$-controlled equalization is explained and discussed on the basis of comparison with current-controlled equalization strategies. Experimental equalization tests emulating partial-shading conditions were performed using the single-switch equalizer employing the $\Delta V$-controlled equalization. Negative impacts of partial-shading were successfully precluded, demonstrating the efficacy of the proposed $\Delta V$-controlled equalization strategy.**

***Index Terms*— Buck-boost converter, partial shading, voltage equalizer, $\Delta V$-controlled equalization.**

## I. Introduction

In order to fully extract power generated by photovoltaic (PV) panels, not only are efficient power converters necessary but also utilization ratio of PV panels should be maximized. Although numerous efficient switching power converters and inverters have been proposed and developed, challenges to improve the solar energy utilization still firmly remain.

A major stumbling block to the improved energy utilization is the partial shading on PV panel/string comprising multiple modules/substrings connected in series (hereafter, simply call module). Since current generated by PV modules are strongly dependent on insolation levels, partial shading on a PV string triggers current mismatch among modules. In a partially-shaded PV string comprising series-connected modules, shaded module(s) is bypassed by bypass diode(s) connected in parallel with it, as shown in Fig. 1(a), resulting in a significant mismatch in operation voltage. These mismatches in current and voltage render the panel to have multiple maximum power points (MPPs), including one global MPP and local MPPs, with which ordinary MPP tracking algorithms cannot perform normally — the partially-shaded panel is likely to operate at its local MPP, a non-optimum operation voltage. Advanced MPPT techniques allow the partially-shaded PV string to operate at its global MPP but shaded module still cannot be fully utilized.

The most straight forward approach to cope with the partial-shading issues is the distributed MPPT system using module-integrated converters (MICs), as shown in Fig. 2(a) [1], [2]. PV modules are individually controlled by respective MICs, overcoming the partial-shading issued. However, the number of

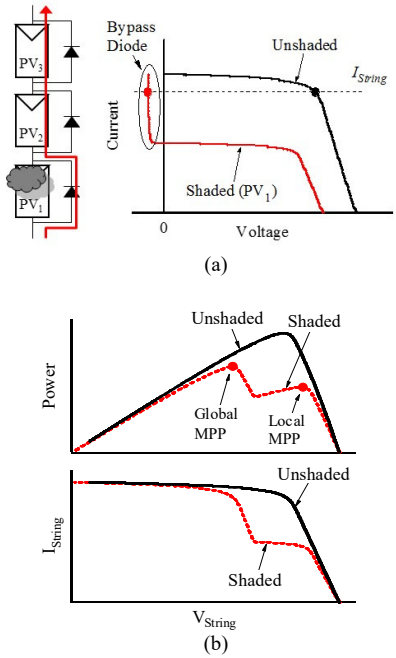


Fig. 1. Influence of partial shading on PV string comprising series-connected modules: (a) PV modules under partial shading condition, (b) String characteristics with/without partial shading.

Manuscript received May 25, 2016, revised July 26, 2016; accepted September 28, 2016. This work was supported by the Ministry of Education, Culture, Sports, Science, and Technology through Grant-in-Aid for Young Scientists (B) 25820118.



M. Uno is with the Faculty of Engineering, Ibaraki University, Hitachi 316-8511, Japan (e-mail: masatoshi.uno.ee@vc.ibaraki.ac.jp).

Akio Kukita is with the Institute of Space and Astronautical Science, Japan Aerospace Exploration Agency, Sagamihara 252-5210, Japan (email: kukita.akio@jaxa.jp).

converters necessary in the distributed MPPT systems is proportional to that of modules, increasing the system cost and complexity. In addition, not only is the efficiency penalty due double power conversion likely but also each MIC needs to be rated with full module power [3], [17]. These are cited as major disadvantages when compared with differential power processing (DPP) converters and voltage equalizers introduced later.

Various kinds of differential power processing (DPP) converters and voltage equalizers have been proposed and developed to address the partial shading issues mentioned above [3]–[26]. With these converters, a fraction of generated power of unshaded modules is transferred to shaded modules so that all the modules are able to operate at the same voltage or even at each MPP [6], [7]. Numerous topologies have been presented, and most of them are based on individual non-isolated bidirectional converters, such as buck-boost converters [3]–[11] and some extended topologies [12]–[14], multi-stage choppers [15], [16], and switched capacitor converters [17]–[19] that provide a power transfer path between adjacent two modules. PV systems employing the adjacent module-to-module equalization is illustrated in Fig. 2(b). In the topologies presented in [20]–[24] [see Fig. 2(c)], each module is equipped with an isolated converter to provide a direct power transfer path between a string and shaded module. In other words, these conventional topologies require multiple converters as well as switches in proportion to the number of modules connected in series. This tendency is considered undesirable from the viewpoints of system and circuit complexity.

Meanwhile, the string-to-module equalization architecture, shown in Fig. 2(d), can reduce the equalizer count, potentially achieving the reduced system cost and complexity. This equalizer is basically a single-input multi-output converter that transfers power from the string to shaded module(s). The two-switch equalizer using an LLC resonant voltage multiplier [25] can be categorized into this architecture. In comparison

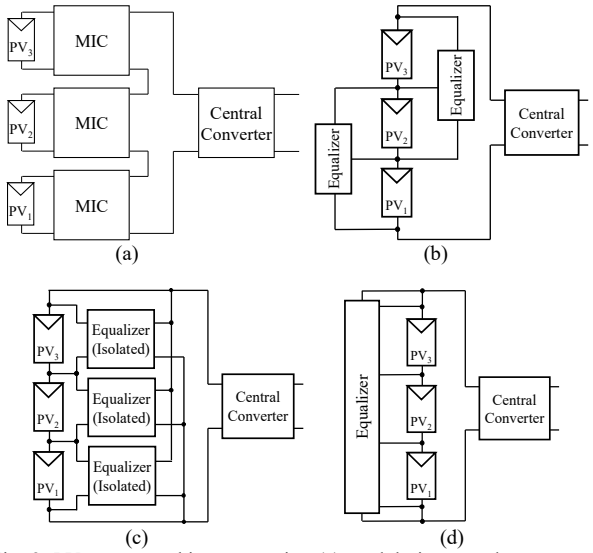


Fig. 2. PV system architectures using (a) module-integrated converters, (b) adjacent module-to-module equalizers, (c) isolated equalizer, and (d) string-to-module equalizer.

with the equalization architectures shown in Figs. 2(b) and (c), the switch count can be dramatically reduced but it still requires two switches, implying there is still room for improvement. The equalizer based on a multi-winding flyback converter [26] is a single-switch topology, but the design difficulty of the multi-winding transformer may arise in practical implementation.

A single-switch voltage equalizer using a multi-stacked buck-boost converters, which had been developed for battery equalization [27], has been proposed for PV strings under partial shading [28]. This equalizer can be derived by stacking multiple capacitor-inductor-diode (C-L-D) filters on a traditional buck-boost converter, such as SEPIC, Zeta, and Ćuk converters. Regardless of the number of modules connected in series, the required switch count is only one, considerably simplifying the circuitry compared to conventional DPP converters and voltage equalizers. However, in order for this equalizer to work optimally, an equalization current supplied to unshaded modules must be controlled to be nearly zero, requiring multiple current sensors in proportion to the number of modules connected in series. From the perspectives of cost and complexity, a current sensorless voltage-based control is preferable to the current-based one.

In our previous work [29], the current sensorless equalization technique was proposed for the single-switch equalizer using the multi-stacked buck-boost converters. This paper presents the fully-developed work about the current sensorless equalization strategy for the single-switch equalizer for PV strings under partial shading. The proposed current sensorless equalization strategy achieves reduced cost and simplified measurement circuit as well as decreased processed power and power conversion loss in the equalizer in comparison with the previously-proposed equalization strategy [28]. In Section II, the circuit topology of the single-switch equalizer is briefly reviewed, and fundamental operation principle of the equalizer employing the current sensorless control technique is explained. The equalization strategy of the current sensorless control is detailed and compared to the conventional equalization strategy in [28] in Section III, followed by the feedback circuit implementation in Section IV. Section V will present experimental results of the equalization tests using the proposed current sensorless equalization strategy. In addition to the detailed analysis and experimental results, potential applications of the proposed $\Delta V$-controlled equalization strategy will be discussed in Section VI.

## II. Single-Switch Voltage Equalizer Using Multi-Stacked Buck-Boost Converters

### A. Topology

By stacking C-L-D filters on a traditional buck-boost converter, such as SEPIC, Zeta, and Ćuk converters, as a foundation, single-switch equalizers can be derived. A SEPIC-based topology for three PV modules $PV_1$–$PV_3$ connected in series is shown in Fig. 3(a), as a representative topology. The input of the SEPIC is tied to the string, while output smoothing capacitors $C_{out1}$–$C_{out3}$ are connected in

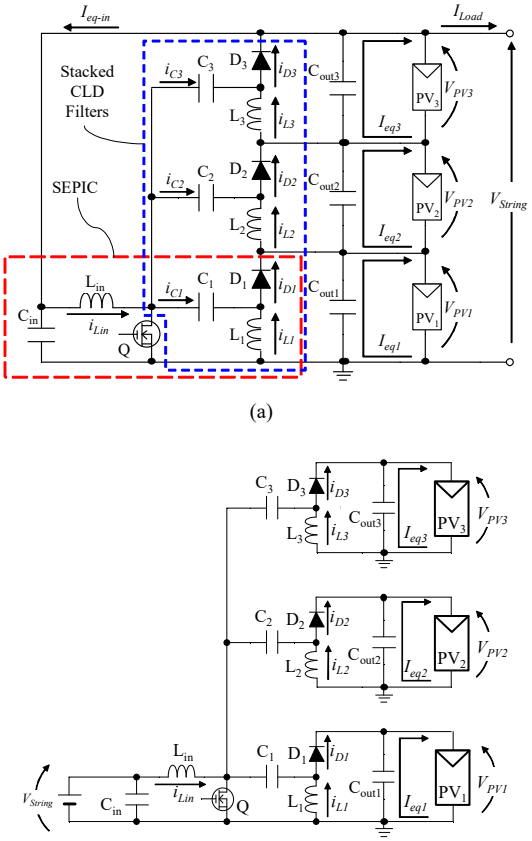


Fig. 3. (a) Single-switch SEPIC-based voltage equalizer and (b) its equivalent circuit.

parallel with $PV_1$–$PV_3$, respectively. A fraction of the generated power of the string is fed to the input of the equalizer. Then, this supplied power is redistributed to shaded modules so that all module voltages are equalized, as will be explained in the following subsection.

### *B. Equivalent Circuit and Mechanism of Voltage Equalization*

A rectangular wave voltage is generated at a switching node of the SEPIC (i.e., the drain of the MOSFET). Since $C_1$–$C_3$ are connected to this switching node, these capacitors can be regarded as coupling capacitors that allow ac components only to flow through them. In other words, C-L-D filters are ac-coupled, suggesting that although $PV_1$–$PV_3$ are at different dc voltage levels, these C-L-D-filters as well as $PV_1$–$PV_3$ can be separated and grounded, as shown in Fig. 3(b).

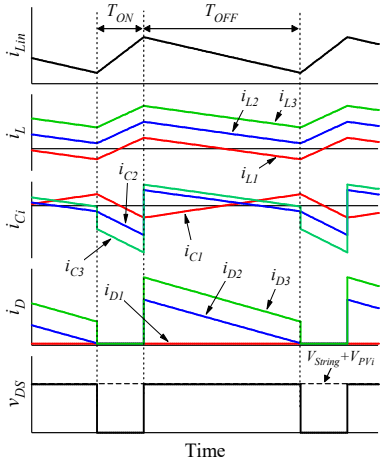


Fig. 4. Key operation waveforms in CCM when $PV_2$ and $PV_3$ are moderately and severely shaded, respectively.

The equivalent circuit shown in Fig. 3(b) provides an intuitive understanding of how module voltages can be automatically equalized under partial shading conditions. All the C-L-D filters as well as $PV_1$–$PV_3$ are equivalently connected in parallel, and therefore, the equalizer preferentially supplies an equalization current to the module having the lowest voltage in a string. In general, a voltage of shaded modules tends to be lower than that of unshaded modules, as illustrated in Fig. 1(a). Hence, equalization currents automatically flow toward shaded modules so that all the module voltages become nearly uniform.

### *C. Fundamental Operation*

Similar to traditional buck-boost converters, the single-switch equalizer operates in either continuous conduction mode (CCM) or discontinuous conduction mode (DCM), depending on the degree of shading. Severely-shaded conditions for the equalizer correspond to heavy loads for traditional converters because large equalization currents are needed to equalize module voltages, and therefore, the equalizer operates in CCM. On the other hand, when the degree of shading is light, the operation likely falls into DCM.

The key operation waveforms in CCM and current flow directions of the equalizer with the current sensorless voltage-based control, which will be proposed and discussed in Section III, are shown in Figs. 4 and 5, respectively. In this case, $PV_2$ and $PV_3$ are moderately and severely shaded, respectively. The waveforms and current flow paths shown in Figs. 4 and 5 are slightly different from those using the previously-proposed

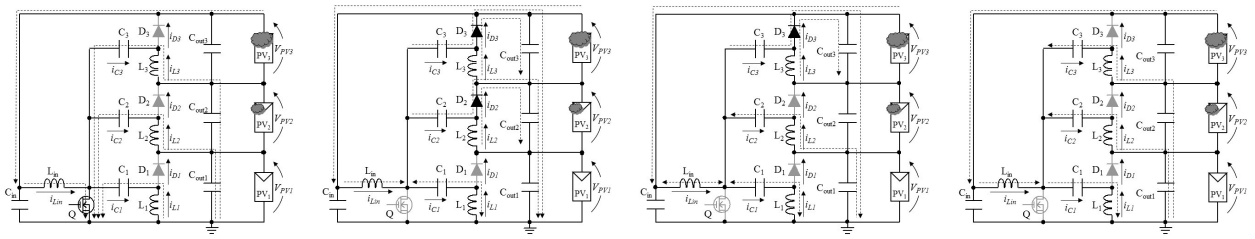


Fig. 5. Current flow directions during (a) $T_{ON}$, (b) $T_{OFF}$ or $T_{OFF\_a}$, (c) $T_{OFF\_b}$, and (c) $T_{OFF\_DCM}$.

current-controlled equalization; with the voltage-based control, the unshaded module $PV_1$ does not receive an equalization current, while equalization currents flow toward all modules when the current-based control is employed [28]. The difference between the current-based and voltage-based controls are detailed in the next section.

In $T_{ON}$ period, the switch Q is turned on, and all the inductor currents, $i_{Lin}$ and $i_{L1}$–$i_{L3}$, linearly increase and flow through Q, as shown in Fig. 5(a). Similar to the traditional SEPIC, voltages applied to inductors $L_{in}$ and $L_i$ (i = 1…3) are equal to the input voltages or the string voltage $V_{String}$.

The operation of the equalizer moves to $T_{OFF}$ period as Q is turned off, and all the inductor currents start linearly decreasing. Applied voltages of inductors are equal to $V^*_{PVi} - V_D$ where $V^*_{PVi}$ is the lowest voltage of shaded modules in the string and $V_D$ is the forward voltage of diodes — $V^*_{PVi} = V_{PV3}$ in the case shown in Figs. 4 and 5. The volt-second balance on inductors under a steady-state condition yields the voltage relationship between $V_{String}$ and $V^*_{PVi}$ as

$$V^*_{PVi} = \frac{D}{1-D} V_{String} - V_D , \quad (1)$$

where $D$ is the duty cycle of the switch Q. $D$ is adjusted so that the voltage difference ($\Delta V$) between the measured highest and lowest module voltages ($V_H$ and $V_L$, respectively) in the string to be a certain fixed value as will be detailed in Section III.

Diodes connected to the shaded modules of $PV_2$ and $PV_3$ (i.e., $D_2$ and $D_3$) conduct, whereas that corresponding to the unshaded module of $PV_1$ ($D_1$) is still off, as shown in Fig. 5(b). From Kirchhoff's current law, an equalization current supplied to $PV_i$, $I_{eqi}$, is equal to an average current of $L_i$ or $D_i$ ($I_{Li}$ or $I_{Di}$) because an average current of $C_i$ must be zero under a steady-state condition;

$$I_{eqi} = I_{Li} = I_{Di} . \quad (2)$$

Since $D_1$ does not conduct under this shading condition, no equalization current is supplied to the unshaded module $PV_1$, and therefore, the average current of $L_1$, $I_{L1}$, is zero although a current ripple exists in $i_{L1}$.

Key operation waveforms in DCM are shown in Fig. 6. The current flow directions in $T_{ON}$ and $T_{OFF\_a}$ in DCM are identical to those in $T_{ON}$ and $T_{OFF}$ in CCM, respectively, while the period of $T_{OFF\_DCM}$ is unique to the DCM operation. In $T_{OFF\_DCM}$ period, all the diode cease to conduct, and all the inductor currents become constant, indicating the applied voltages of inductors are zero.

Similar to the CCM, the voltage relationship between $V_{String}$ and $V^*_{PVi}$ can be expressed as

$$V^*_{PVi} = \frac{D}{D_{ab}} V_{String} - V_D , \quad (3)$$

where $D_{ab}$ is the duty cycle of the sum of $T_{OFF\_a}$ and $T_{OFF\_b}$ periods in DCM, as designated in Fig. 6. The boundary between CCM and DCM can be established based on whether all diode currents reach zero in switch-off state. In other words, if $D_{ab}$ is shorter than $1 - D$ (i.e., $D_{ab} < 1 - D$), the operation falls into DCM. The critical duty cycle $D_{Critical}$ can be yielded as

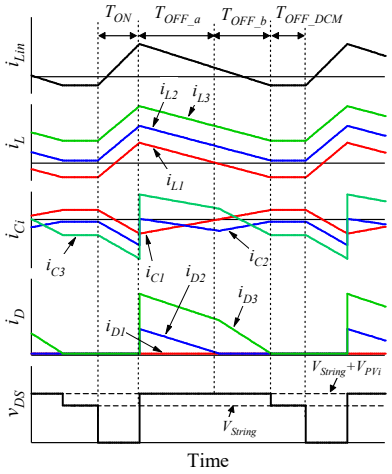


Fig. 6. Key operation waveforms in DCM when $PV_2$ and $PV_3$ are moderately and severely shaded, respectively.

$$D_{Critical} = \frac{V^*_{PVi} + V_D}{V_{String} + V_{PVi} + V_D} . \quad (4)$$

## III. Equalization Strategy

In order to effectively preclude the negative impacts caused by partial shading, the equalizer needs to be properly controlled with minimizing power conversion loss in the equalizer. Although voltage equalization does not guarantee that all the modules operate at each MPP, the loss in energy yield is reportedly satisfactory small and less than 2% below the ideal individual MPPT [23]. Hence, equalization strategy discussed in this section is aimed for voltage equalization.

The proposed single-switch equalizer is basically a single-input multi-output power source with one control freedom (i.e., duty cycle). In order to equalize (or supply equalization currents to) multiple PV modules with single one control freedom, the equalizer should be operated with a proper equalization strategy. Depending on strategies, there are three conceivable equalization scenarios (see Fig. 7) that are considered in this section. This section deals with a partial shading condition where $PV_2$ and $PV_3$ are moderately and severely shaded, respectively, similar to the case discussed in the previous section. For the sake of clarity, the equalizer is illustrated as a multi-output power source of $V_e$ having respective equivalent output resistors $R_{out}$ and output diodes. From Fig. 7, the relationship between the shaded module's voltage $V^*_{PVi}$ and $V_e$ can be yielded as

$$V^*_{PVi} = V_e - I_{eqi} R_{out} - V_D . \quad (5)$$

From (1) and (5),

$$V_e = \frac{D}{1-D} V_{String} - I_{eqi} R_{out} \approx \frac{D}{1-D} V_{String} , \quad (6)$$

indicating that $V_e$ is essentially duty-controllable.

### A. Equalization Scenarios

In the first scenario, the over-equalization scenario shown in Fig. 7(a), equalization currents are supplied to all modules including the unshaded module $PV_1$; a difference between

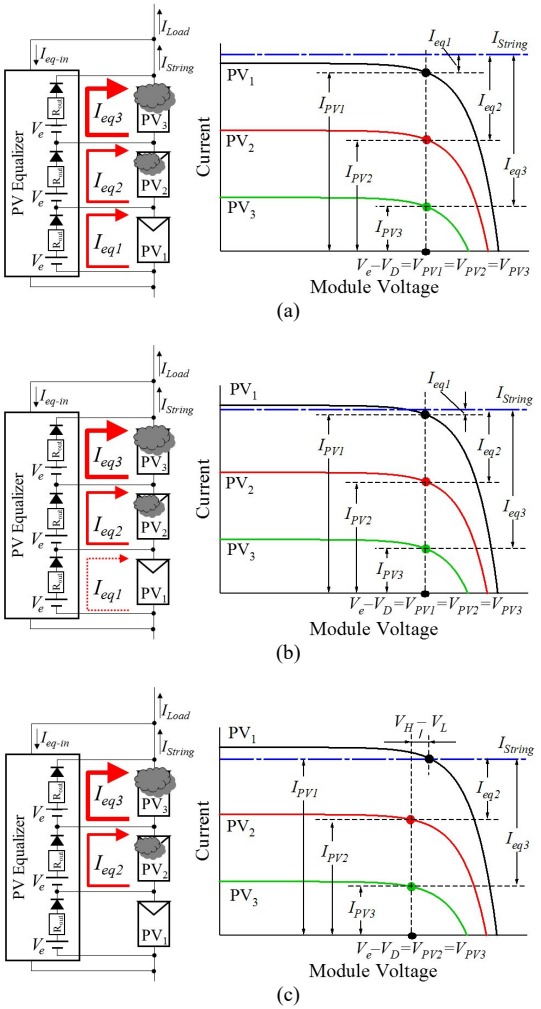


Fig. 7. Equalization scenarios: (a) Over-equalization, (b) current-controlled equalization, and (c) current sensorless $\Delta V$-controlled equalization.

IString and $I_{PVi}$ corresponds to an equalization current $I_{eqi}$, as designated in the figure. Since all the output diodes of the equalizer conduct, all the module voltages are equalized as $V_e - V_D = V_{PVi}$ if voltage drops across $R_{out}$ are neglected. However, the unshaded module $PV_1$ unnecessarily receives an equalization current, increasing the processed power as well as power conversion loss in the equalizer.

In the current-controlled equalization scenario, which is shown in Fig. 7(b) and has been previously employed for the single-switch equalizer [28], the unnecessary equalization current for the unshaded module $PV_1$ is minimized. Similar to the over-equalization scenario, all the output diodes of the equalizer conduct, equalizing all the module voltages as $V_e - V_D = V_{PVi}$. In addition, the minimized unnecessary equalization current for the unshaded module reduces the processed power as well as the power conversion loss in the equalizer. However, in order to minimize the unnecessary equalization current for the unshaded module, this equalization current needs to be measured and controlled using a current sensor, which is not desirable from the cost perspective. Besides, the current-controlled equalization strategy requires multiple current sensors in proportion to the module count because all

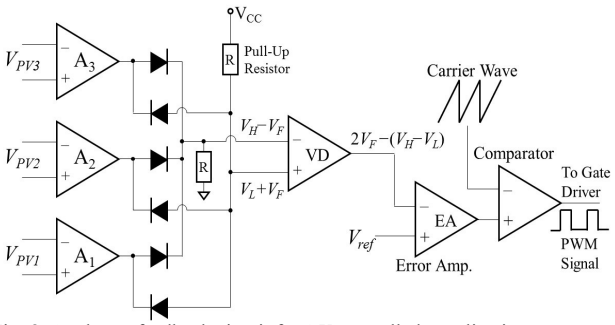


Fig. 8. Analogue feedback circuit for $\Delta V$-controlled equalization.

modules are potentially shaded and receive the controlled minimized equalization current, depending on partial shading conditions in practical use.

In the third equalization scenario, the voltage-difference-controlled equalization scenario (hereafter, simply call $\Delta V$-controlled equalization), module voltages are 'nearly' equalized without measuring the equalization current for the unshaded module, and therefore, it is essentially a current sensorless equalization method. Instead of currents, the voltage difference between the modules having the highest and lowest voltages ($V_H$ and $V_L$) is controlled, as shown in Fig. 7(c). Equalization currents are supplied to shaded modules only, and their voltages are equalized as $V_{PV2} = V_{PV3} = V_e - V_D = V_L$ —the voltage drops across $R_{out}$ is ignored —, while the unshaded module $PV_1$ receives no equalization current and the output diode for $PV_1$ does not conduct because $V_{PV1}$ is higher than $V_e - V_D$. In other words, $V_L$ (= $V_{PV2}$ = $V_{PV3}$ = $V_e$ − $V_D$) is duty-controllable as (5) and (6) indicate, while $V_H$ (= $V_{PV1}$) is independent on duty cycle, and therefore, the voltage difference of $V_H - V_L = \Delta V$ can be adjusted by duty cycle —$\Delta V$ decreases with an increase in duty cycle. In the $\Delta V$-controlled equalization scenario, the equalizer operates so that $\Delta V$ is controlled to be a certain fixed value as will be discussed in Section III-C.

### *B. Features of $\Delta V$-Controlled Equalization*

In comparison with the previously-reported control strategy using multiple current sensors in proportion to the number of modules [28], the proposed $\Delta V$-controlled equalization is current sensorless, therefore achieving reduced cost and dramatic simplification in measurement circuits by eliminating current sensors.

In addition, the $\Delta V$-controlled equalization can reduce power conversion loss by completely eliminating the unnecessary equalization current for the unshaded modules. With the previously-reported equalization strategy [28], an equalization current unnecessarily flows to unshaded module $PV_1$ [see Fig. 7(b)], increasing the processed power and conversion loss in the equalizer. With the $\Delta V$-controlled equalization, on the other hand, no equalization current flows toward the unshaded module $PV_1$ [see Fig. 7(c)], hence reducing the processed power as well as power conversion loss in the equalizer.

However, module voltages with the proposed $\Delta V$-controlled equalization cannot be completely equalized because of the existence of $\Delta V = V_H - V_L$. This incomplete voltage

equalization might lead to a decreased energy yield, especially when the value of $\Delta V$ is set large. However, by setting the value of $\Delta V$ to be small enough compared with module voltages, all the module voltages can be adequately equalized without significantly degrading the energy yield from the PV string under partial shading conditions.

### C. Determination of $\Delta V$ for $\Delta V$-Controlled Equalization

The value of $\Delta V$ needs to be determined considering noise and an equivalent output resistance, which was neglected in the previous subsection for the sake of clarity. In the case of Fig. 7(c), module voltages, $V_{PV1}$–$V_{PV3}$, are expressed as

$$\begin{cases} V_{PV1} \geq V_e - V_D \\ V_{PV2} = V_e - V_D - I_{eq2} R_{out} \\ V_{PV3} = V_e - V_D - I_{eq3} R_{out} \end{cases}, \quad (7)$$

where $R_{out}$ is the equivalent resistance value. By defining shaded and unshaded module voltages as $V_{Shaded}$ and $V_{Unshaded}$, respectively, (7) can be arranged as

$$V_{Unshaded} \geq V_{Shaded} + I_{eq} R_{out} . \quad (8)$$

In the $\Delta V$-controlled equalization, $\Delta V$ (= $V_H$ − $V_L$) corresponds to the voltage difference of $V_{Shaded}$ and $V_{Unshaded}$, and therefore,

$$\Delta V \geq I_{eq} R_{out} . \quad (9)$$

This equation suggests that $\Delta V$ must be determined considering $R_{out}$ and potentially largest equalization current $I_{eq}$ so that no equalization current flows toward unshaded modules.

## IV. Feedback Circuit Implementation

The proposed current sensorless $\Delta V$-controlled equalization strategy can be implemented by either an analogue or digital control circuit. In this paper, an analogue feedback circuit was employed.

The analogue feedback circuit for $\Delta V$-controlled equalization is shown in Fig. 8. All the module voltages are individually measured using operational amplifiers $A_1$–$A_3$. Outputs of $A_1$–$A_3$ are connected in parallel through respective output diodes and are tied to the inputs of the differential amplifier VD so that the highest and the lowest module voltages (i.e., $V_H$ and $V_L$) in the string are inputted to the inverting and non-inverting inputs of the VD, respectively; $V_H - V_F$ and $V_L + V_F$ are inputted to the inverting and non-inverting inputs, respectively, where $V_F$ is the forward voltage drop of diodes in the feedback circuit. Hence, VD outputs $2V_F - (V_H - V_L)$ for the error amplifier to generate a PWM signal in the comparator stage. Therefore, with the known value of $V_F$, the voltage difference $\Delta V$ (= $V_H$ − $V_L$) can be arbitrary determined by properly setting $V_{ref}$.

Table I
Component values for the prototype.

| Component | Value |
|---|---|
| $C_1$–$C_3$ | Ceramic Capacitor, 44 µF, 5 mΩ |
| $C_{out1}$–$C_{out3}$ | Ceramic Capacitor, 141 µF |
| $D_1$–$D_3$ | PDS4150, $V_D$ = 0.71 V |
| $L_{in}$ | 82 µH, 87.3 mΩ |
| $L_1$–$L_3$ | 68 µH, 72.1 mΩ |
| Q | FDS86240, $R_{DS}$ = 35.3 mΩ |

## V. Experimental Results

### A. Prototype and its Output Resistance

A 75-W prototype for three modules connected in series was built and its component values are listed in Table I. The measured average power conversion efficiency of the prototype operating at a switching frequency of 170 kHz was approximately 90%.

The output resistance $R_{out}$ was measured with the experimental setup shown in Fig. 9(a). The equalizer was fed by an external voltage-source power supply, while PV modules were removed and a variable resistor was connected in parallel with $C_{out1}$. The prototype was operated at a fixed duty cycle of $D$ = 0.25.

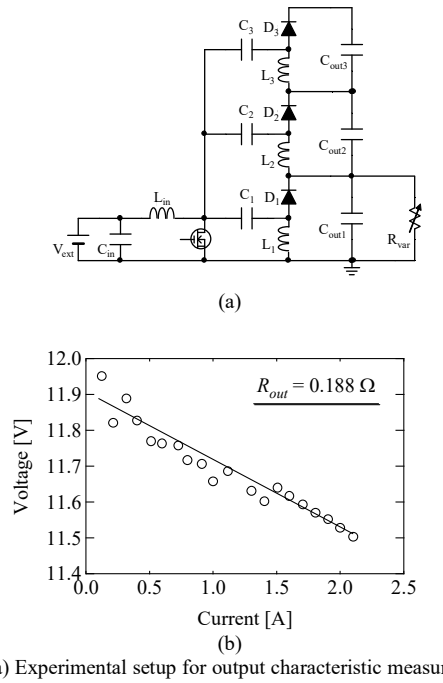


Fig. 9. (a) Experimental setup for output characteristic measurement and (b) measured output characteristic.

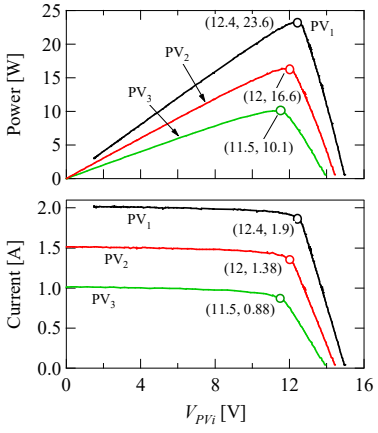


Fig. 10. Individual module characteristics used for the first partial shading case.

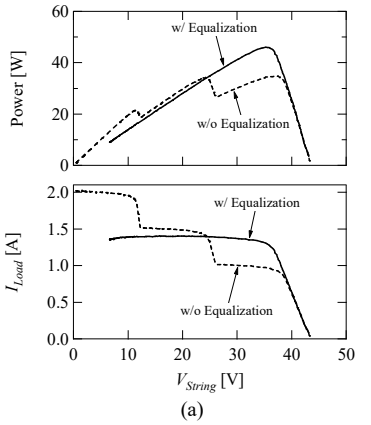


Fig. 11. Experimental results in the first partial shading case: (a) String characteristics with/without equalization, (b) individual module characteristics with equalization.

The measured output characteristic of the prototype is shown in Fig. 9(b). From the slope of the measured *V–I* characteristic, the value of $R_{out}$ was calculated to be 0.188 Ω. Assuming the potentially largest $I_{eq}$ is 1.0 A with considering the influence of noise, the value of $\Delta V$ was determined to be 300 mV according to (9).

### *B. Equalization Tests Emulating Partial Shading Conditions*

Solar array simulators (Agilent Technology, E4360A) were used to emulate two partial shading conditions. The equalizer was controlled using the feedback circuit shown in Fig. 8 for the current sensorless $\Delta V$-controlled equalization with $\Delta V$ = 300 mV. A resistance of an electronic load connected to the string was manually varied in order to sweep the string characteristics with/without the equalizer.

Individual module characteristics used for the first partial shading case are shown in Fig. 10; $PV_2$ and $PV_3$ are moderately and severely shaded, respectively, similar to the case taken in Sections II and III. The measured string characteristics with/without the equalizer are compared in Fig. 11(a). Three MPPs, including one global and two local MPPs, were observed when without equalization, and the extractable maximum power was merely 34 W at $V_{String}$ = 24 V. Meanwhile, with the equalizer, the local MPPs successfully disappeared and the extractable maximum power increased to as high as 46 W at $V_{String}$ = 35 V. This result indicates that 92% of the string power

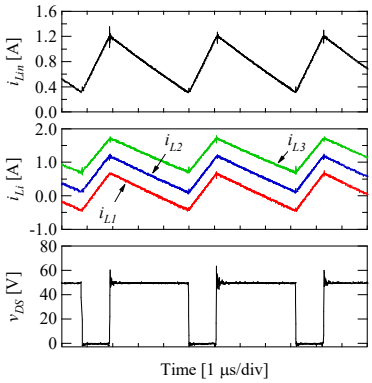


Fig. 12. Measured waveforms in the first partial-shading case.

was extracted with the support of the equalizer, and the rest 8% of the string power was dissipated in the form of power conversion loss in the equalizer and/or was not extracted because voltage equalization does not guarantee that all the modules operate at each MPP.

The measured individual module characteristics with the equalizer are shown in Fig. 11(b). All the module characteristics were nearly unified by the support of the equalizer. The voltage difference between the highest and lowest module voltages was controlled to be approximately 300 mV.

Measured key waveforms at $V_{String}$ = 35 V are shown in Fig. 12. The average current of $i_{L2}$ and $i_{L3}$ were higher than zero, depending on the degree of shading, while that of $i_{L1}$ was zero, suggesting no equalization current was supplied to the unshaded module $PV_1$ — an equalization current flowing to a module is equal to an average current of corresponding inductor, as expressed by (2).

The experimental equalization test for the second case was performed emulating a slightly-shaded condition so that the equalizer operates in DCM. The individual module characteristics used for the second partial shading case are shown in Fig. 13.

The measured string characteristics with/without the equalizer are shown and compared in Fig. 14(a). Similar to the

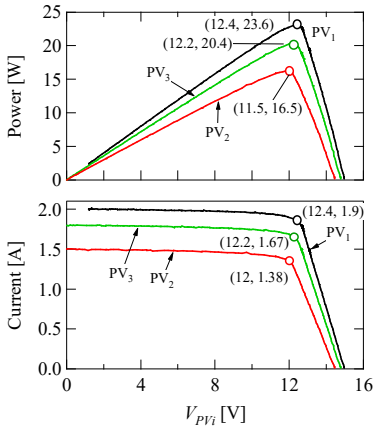


Fig. 13. Individual module characteristics used for the second partial shading case.

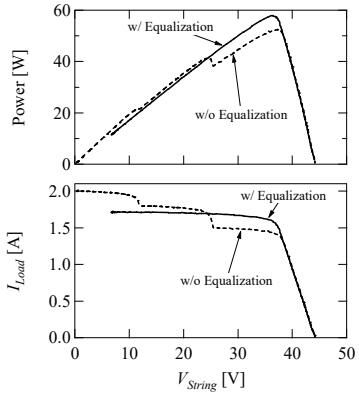


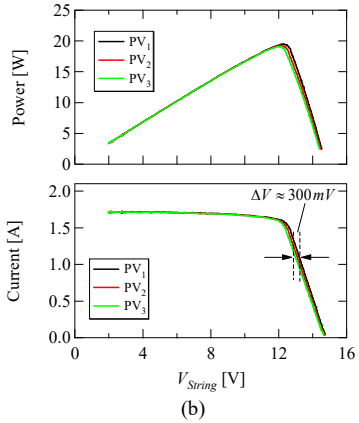


Fig. 14. Experimental results in the second partial shading case: (a) String characteristics with/without equalization, (b) individual module characteristics with equalization.

first experiment, the local MPPs were successfully eliminated by the equalizer, and the extractable maximum power was increased to 57.9 W which accounts for 95.7% of the string power. The measured individual module characteristics with the equalizer operating in DCM are shown in Fig. 14(b). Similar to the first case, the module voltages were successfully uniformed within 300 mV even in DCM condition.

The measured waveforms in the second partial shading case are shown in Fig. 15. All inductor currents were discontinuous triangular waves, and voltage oscillation caused by resonance between the output capacitance of the MOSFET and inductors was observed in the drain-source voltage $v_{DS}$. The average of $i_{L1}$ was zero while those of $i_{L2}$ and $i_{L3}$ were substantial, indicating that the equalizer supplied no equalization current for the unshaded module $PV_1$ even in DCM operation. These results demonstrate the efficacy of the proposed $\Delta V$-controlled equalization under both CCM and DCM operations.

## VI. Application of $\Delta V$-Controlled Equalization to Other Equalizers

The $\Delta V$-controlled equalization strategy has been proposed for the single-switch equalizer that is equivalently a multi-output power source with one control freedom, as mentioned at the beginning of Section III. The proposed $\Delta V$-controlled equalization can be applied to other voltage

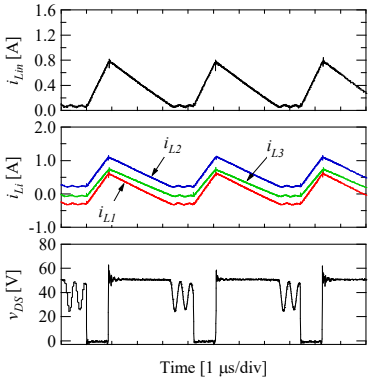


Fig. 15. Measured waveforms in the second experiment.

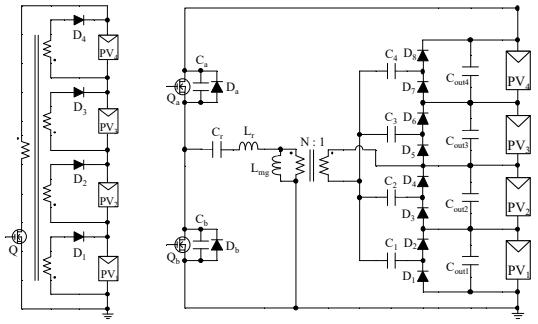


Fig. 16. (a) Single-switch equalizer based on multi-winding flyback converter [26], (b) two-switch equalizer using LLC resonant voltage multiplier [25].

equalizers that are equivalently a multi-output power source with one control freedom. For instance, the single-switch equalizer based on the multi-winding flyback converter [26], as shown in Fig. 16(a), is a duty-controlled multi-output power source. Another example is the two-switch voltage equalizer using an LLC resonant voltage multiplier [25] shown in Fig. 16(b) that is a frequency-controlled multi-output power source. Both equalizer can be equivalently expressed as the multi-output power source of $V_e$ having equivalent output resistance Rout and output diodes, as illustrated in Fig. 7. Although open-loop control may be feasible (e.g., as reported in [25]), the $\Delta V$-controlled equalization would improve the equalization performance of these equalizer.

## VII. Conclusions

The single-switch equalizer presented in this paper can reduce the switch count compared to conventional topologies, achieving simplified circuitry. However, with a previously-employed current-controlled equalization strategy, the number of current sensors necessary is proportional to the module count, likely resulting in increased cost and complexity of a feedback circuit.

Three equalization strategies, including the previously-employed current-controlled equalization and proposed current sensorless $\Delta V$-controlled equalization, were compared and discussed. The $\Delta V$-controlled equalization was

concluded to be a preferable equalization strategy because of the lack of current sensors while achieving a reasonable equalization performance.

Experimental equalization tests emulating partial shading conditions were performed using the single-switch equalizer employing the proposed $\Delta V$-controlled equalization. With the support of the equalizer, local MPPs were successfully eliminated and the extractable maximum power was significantly improved. All the module voltages were nearly unified, demonstrating the efficacy of the proposed current sensorless $\Delta V$-controlled equalization.

## REFERENCES


[1] M.Vitelli, "On the necessity of joint adoption of both distributed maximum power point tracking and central maximum power point tracking in PV systems," *Prog. Photovoltaic Res. Appl*., vol. 22, pp. 283–299, 2014.

[2] S. Poshtkouhi, V. Palaniappan, M. Fard, and O. Trescases, "A general approach for quantifying the benefit of distributed power electronics for fine grained MPPT in photovoltaic applications using 3-D modeling," *IEEE Trans. Power Electron*., vol. 27, no. 11, pp. 4656–4666, Nov. 2012.

[3] P. S. Shenoy, K. A. Kim, B. B. Johnson, and P. T. Krein, "Differential power processing for increased energy production and reliability of photovoltaic systems," *IEEE Trans. Ind. Power Electron*., vol. 28, no. 6, pp. 2968–2979, Jun. 2013.

[4] H. J. Bergveld, D. Büthker, C. Castello, T. Doorn, A. D. Jong, R. V. Otten, and K. D. Waal, "Module-level dc/dc conversion for photovoltaic systems: the delta-conversion concept," *IEEE Trans. Power Electron*., vol. 28, no. 4, pp. 2005–2013, Apr. 2013.

[5] M. S. Zaman, Y. Wen, R. Fernandes, B. Buter, T. Doorn, M. Dijkstra, H. J. Bergveld, and O. Trescases, "A cell-level differential power processing IC for concentrating-PV systems with bidirectional hysteretic current-mode control and closed-loop frequency regulation," *IEEE Trans. Power Electron*., vol. 28, no. 6, pp. 2936–2945, Jun. 2013.

[6] S. Qin and R. C. N. P. Podgurski, "Sub-module differential power processing for photovoltaic applications," in Proc. *IEEE Applied Power Electron. Conf. Expo*., pp. 101–108, 2013.

[7] S. Qin, S. T. Cady, A. D. D. García, and R. C. N. P. Podgurski, "A distributed approach to MPPT for PV sub-module differential power processing," in Proc. *IEEE Energy Conversion Conf. Expo*., pp. 2778–2785, 2013.

[8] R. Kadri, J. P. Gaubert, and G. Champenois, "New converter topology to improve performance of photovoltaic power generation system under shading conditions," in Proc. *Int. Conf. Power Eng. Energy Electrical Drives*, pp. 1–7, 2011.

[9] R. Kadri, J. P. Gaubert, and G. Champenois, "Centralized MPPT with string current diverter for solving the series connection problem in photovoltaic power generation system," in Proc. *Int. Conf. Power Eng. Energy Electrical Drives*, pp. 116–123, 2011.

[10] R. Giral, C. A. R. Paja, D. Gonzalez, J. Calvente, À. C. Pastpr, and L. M. Salamero, "Minimizing the effects of shadowing in a PV module by means of active voltage sharing," in Proc. *IEEE Int. Conf. Ind. Technol*, pp. 943–948, 2010.

[11] R. Giral, C. E. Carrejo, M. Vermeersh, A. J. Saavedra-Montes, and C. A. Ramos-Paja, "PV field distributed maximum power point tracking by means of an active bypass converter," in Poc. *Int. Conf. Clean Electrical Power*, pp. 94–98, 2011.

[12] L. F. L. Villa, T. P. Ho, J. C. Crebier, and B. Raison, "A power electronics equalizer application for partially shaded photovoltaic modules," *IEEE Trans. Ind. Electron*., vol. 60, no. 3, pp. 1179–1190, Mar. 2013.

[13] L. F. L. Villa, X. Pichon, F. S. Ardelibi, B. Raison, J. C. Crebier, and A. Labonne, "Toward the design of control algorithms for a photovoltaic equalizer: choosing the optimal switching strategy and the duty cycle," *IEEE Power Electron*., vol. 29, no. 3, pp. 1447–1460, Mar. 2014.

[14] M. Z. Ramli and Z. Salam, "A simple energy recovery scheme to harvest the energy from shaded photovoltaic modules during partial shading," *IEEE Tran. Power Electron*., vol. 29, no. 12, pp. 6458–6471, Dec. 2014.

[15] T. Shimizu, O, Hashimoto, and G. Kimura, "A novel high-performance utility-interactive photovoltaic inverter system," *IEEE Trans. Power Electron*., vol. 18, no. 2, pp. 704–711, Mar. 2003.

[16] T. Shimizu, M. Hirakata, T. Kamezawa, and H. Watanabe, "Generation control circuit for photovoltaic modules," *IEEE Trans. Power Electron*., vol. 16, no. 3, pp. 293–300, May 2001.

[17] J. T. Stauth, M. D. Seeman, and K. Kesarwani, "Resonant switched-capacitor converters for sub-module distributed photovoltaic power namagement," *IEEE Trans. Power Electron*., vol. 28, no. 3, pp. 1189–1198, Mar. 2013.

[18] R. Sangwan, K. Kesarwani, and J. T. Stauth, "High-density power converters for sub-module photovoltaic power management," in Proc. *IEEE Energy Conversion Cong. Expo*., pp. 3279–3286, 2014.

[19] S. B. Yaakov, A. Blumenfeld, A. Cervera, and M. Evzelman, "Design and evaluation of a modular resonant switched capacitor equalizer for PV panels," in Proc. *IEEE Energy Conversion Cong. Expo*., pp. 4129–4136, 2012.

[20] Y. Nimni and D. Shmilovitz, "Returned energy architecture for improved photovoltaic systems efficiency," in Proc. *IEEE Int. Symp. Circuit Syst*., pp. 2191–2194, 2010.

[21] C. Olalla, M. Rodríguez, D. Clement, J. Wang, and D. Makisimović, "Architecture and control of PV modules with submodule integrated converter," in Proc. *IEEE Control and Modeling for Power Electron*., pp. 1–6, 2012.

[22] C. Olalla, D. Clement, M. Rodríguez, and D. Makisimović, "Architectures and control of submodule integrated dc-dc converters for photovoltaic applications," *IEEE Trans. Power Electron*., vol. 28, no. 6, pp. 2980–2997, Jun. 2013.

[23] C. Olalla, C. Deline, D. Clement, Y. Levron, M. Rodríguez, and D. Makisimović, "Performance of power limited differential power processing architectures in mismatched PV systems," *IEEE Trans. Power Electron*., vol. 30, no. 2, pp. 618–631, Feb. 2015.

[24] Q. Zhang, X. Sun, Y. Zhong, and M. Matui, "A novel topology for solving the partial shading problem in photovoltaic power generation system," in Proc. *IEEE Power Electron. Motion Cont. Conf*., pp. 2130–2135, 2009.

[25] M. Uno and A. Kukita, "Two-switch voltage equalizer using an LLC resonant inverter and voltage multiplier for partially-shaded series-connected photovoltaic modules," *IEEE Trans. Ind. Appl*., vol. 51, no. 2, Mar/Apr. 2015, pp. 1587–1601.

[26] J. Du, R. Xu, X. Chen, Y. Li, and J. Wu, "A novel solar panel optimizer with self-compensation for partial shadow condition," in Proc. *IEEE Applied Power Electron. Conf. Expo*., pp. 92–96, 2013.

[27] M. Uno and K. Tanaka, "Single-switch cell voltage equalizer using multistacked buck–boost converters operating in discontinuous conduction mode for series-connected energy storage cells," *IEEE Trans. Veh. Technol*., vol. 60, no. 8, Oct. 2011, pp. 3635–3645.

[28] M. Uno and A. Kukita, "Single-switch voltage equalizer using multi-stacked buck-boost converters for partially-shaded photovoltaic modules," *IEEE Trans. Power Electron*., vol. 30, no. 6, Jun. 2015, pp. 3091–3105.

[29] M. Uno and A. Kukita, "Current sensorless single-switch voltage equalizer using multi-stacked buck-boost converters for photovoltaic modules under partial shading," in Proc. *IEEE Int. Conf. Power Electron. (ICPE), ECCE-Asia*, pp. 1889–1896, Jun. 2015.


**Masatoshi Uno** (M'06) was born in Japan in 1979. He received the B.E. degree in electronics engineering and the M.E. degree in electrical engineering from Doshisha University, Kyoto, Japan, and the Ph.D. degree in space and astronautical science from the Graduate University for Advanced Studies, Hayama, Japan, in 2002, 2004, and 2012, respectively. In 2004, he joined the Japan Aerospace Exploration Agency, Sagamihara, Japan, where he developed spacecraft power systems including battery, photovoltaic, and fuel cell systems. In 2014, he joined the Department of Electrical and Electronics Engineering, Ibaraki University, Ibaraki, Japan, where he is currently an Associate Professor of Electrical Engineering. His research interests include switching power converters, cell equalizers, life evaluation for supercapacitors and lithium-ion batteries, and development of fuel cell systems. Dr. Uno is a member of the Institute of Electrical Engineers of

Japan (IEEJ) and the Institute of Electronics, Information, and Communication Engineers (IEICE).

M. Uno is a member of the Institute of Electrical Engineering of Japan (IEEJ), and the Institute of Electronics, Information and Communication Engineers (IEICE).

**Akio Kukita** was born in Japan in 1967. He received the B.E. degree in physics from Chuo University, Japan, in 1993. From 1993 to 1996 and 1996 to 2008, he was with SEIKO Holdings Corporation and Ebara Corporation, respectively. Since 2008, he has been with Japan Aerospace Exploration Agency as a senior engineer. His recent work has focused on the development of spacecraft power systems.